

Article

# The Effect of Surfactant Content over Cu-Ni Coatings Electroplated by the sc-CO<sub>2</sub> Technique

Ho-Chiao Chuang \*, Jorge Sánchez and Hsiang-Yun Cheng

Department of Mechanical Engineering, National Taipei University of Technology, Taipei 10608, Taiwan; t103569010@gmail.com (J.S.); mark155214155214@yahoo.com.tw (H.-Y.C.)

\* Correspondence: hchuang@mail.ntut.edu.tw; Tel.: +886-2-2771-2171 (ext. 2076)

Academic Editor: Federico Bella

Received: 15 March 2017; Accepted: 18 April 2017; Published: 19 April 2017

**Abstract:** Co-plating of Cu-Ni coatings by supercritical CO<sub>2</sub> (sc-CO<sub>2</sub>) and conventional electroplating processes was studied in this work. 1,4-butyne-1,3-diol was chosen as the surfactant and the effects of adjusting the surfactant content were described. Although the sc-CO<sub>2</sub> process displayed lower current efficiency, it effectively removed excess hydrogen that causes defects on the coating surface, refined grain size, reduced surface roughness, and increased electrochemical resistance. Surface roughness of coatings fabricated by the sc-CO<sub>2</sub> process was reduced by an average of 10%, and a maximum of 55%, compared to conventional process at different fabrication parameters. Cu-Ni coatings produced by the sc-CO<sub>2</sub> process displayed increased corrosion potential of ~0.05 V over Cu-Ni coatings produced by the conventional process, and 0.175 V over pure Cu coatings produced by the conventional process. For coatings ~10 μm thick, internal stress developed from the sc-CO<sub>2</sub> process were ~20 MPa lower than conventional process. Finally, the preferred crystal orientation of the fabricated coatings remained in the (111) direction regardless of the process used or surfactant content.

**Keywords:** supercritical CO<sub>2</sub>; electroplating; 1,4-butyne-1,3-diol; Cu-Ni coating; internal stress; electrochemical resistance

## 1. Introduction

Cu and Cu-rich alloys are popular engineering materials due to their many technological and metallurgical uses. However, Cu is a relatively soft metal with poor chemical properties for some applications, so efforts are being made to solve these issues. One such solution is alloying Cu with Ni; the addition of even small quantities of Ni effectively enhances the mechanical and chemical properties of pure Cu. The earliest research reported for this topic was on Monel alloys [1], which present good ductility and thermal conductivity. Cu-Ni alloys are important engineering materials due to their characteristic mechanical, magnetic, electrochemical, and electrocatalytic properties [2]. Nowadays, many industrial applications rely on Cu-Ni alloys; they are desirable for highly-corrosive environments, such as marine and microbiological applications. Moreover, resistance to pitting corrosion, crevice corrosion, and stress corrosion is desired for high-temperature applications [3]. Cu-Ni alloy coatings with various compositions are used in the microelectronics industry and in portable electronics such as integrated circuits, personal computers, and cellphones. However, an issue with Cu-Ni co-plating is the relatively large difference in electric potential for chemical reduction, ranging from +0.35 vs. a standard hydrogen electrode (SHE) to −0.25 vs. SHE. To perform direct current (DC) electroplating with no surfactants, a relatively higher current density is required. Consequently, increasing current density results in surface defects, causing different issues. Thus, efforts should be focused on the improvement of the electroplating process at low DC settings.

Baskaran et al. [4] performed experiments using pulse electroplating, adjusting the current density, and studied the effects of heat treatment over their samples; they found that the composition

of Cu-Ni alloy could be affected by changes in current density applied during electroplating. Alper et al. [5] reported electroplating using a three-electrode setup supplying negative potential and adjusting pH values, which affected the surface morphology and magnetic properties of the samples. Desislava et al. [6] studied the Hull cell electroplating method, discussing the differences in surface morphology and the degree of influence over the grain size by adjusting Cu and Ni ion concentrations in solution and the current density. Moreover, it has been shown that additives can change the properties of coatings and some even reduce the internal stress in thin films [7].

1,4-butyne-1,3-diol is an additive frequently used to obtain metal deposits with fine grains, bright surfaces, and it provides a levelling effect under the Watt's bath electrolyte process [8]. Atanassov et al. [9] studied the effect of butyne-1,3-diol over Ni coatings. 1,4-butyne-1,3-diol contains hydroxyl groups, OH, which can act as a base towards  $H^+$  ions, reacting with them in solution, allowing the cathode to produce a negative shift in potential. Consequently, Ni was co-plated with Cu. Additionally, as a type of gemini surfactant, 1,4-butyne-1,3-diol, with an ideal solution interface adsorption capacity, can depress rapid accumulation of  $H^+$  and simultaneously promote the migration rate of  $H^+$  from the cathode to the solution interface [10].

Even though adding 1,4-butyne-1,3-diol makes the plated surfaces smoother, the conventional process showed a disadvantage when the sample surface has a complex morphology. This reduces the ability of the electrolyte to flow smoothly, increases viscosity, and creates residual  $H^+$  in the coating during electroplating. Residual  $H^+$  can create defects, such as pinholes [11], which increase surface roughness, internal stresses, and reduce corrosion resistance. Some studies have reported  $sc-CO_2$  mixed with common electroplating solution, resulting in coatings with the following characteristics: (1) finer grains; (2) smoother surfaces; (3) increased wear resistance; and (4) increased corrosion resistance [12–16].  $sc-CO_2$  electroplating for both Cu and Ni have become increasingly popular in the past decades for fabrication of coatings and structures because of superior coverage capabilities and enhanced mechanical properties provided to the electroplated metal [12,17]. The introduction of additives, such as 1,4-butyne-1,3-diol, to the electrolyte and the  $sc-CO_2$  electroplating process both present advantages over the conventional electroplating process for the deposition of Cu-Ni coatings, however, there is no reports in the literature discussing co-plating of Cu-Ni alloys under  $sc-CO_2$  electroplating with the addition of 1,4-butyne-1,3-diol. 1,4-butyne-1,3-diol can be considered an effective surfactant in this context, because by reducing localized concentrations of  $H^+$  in solution it promotes emulsification between the  $sc-CO_2$  and electrolyte.

In this work, 1,4-butyne-1,3-diol was introduced to the  $sc-CO_2$  electroplating process to reduce both internal stresses and surface roughness, and to study the co-plating of Cu-Ni coatings under a pressure of 15 MPa and temperature of 50 °C. Various analyses of mechanical and chemical properties were performed, which will be described in more detail in the sections below.

## 2. Experimental

### 2.1. Materials and System Configuration

The anode used in this study was a piece of Pt with dimensions 20 mm × 20 mm × 0.2 mm. The cathode used in this study was a circular slab of brass with a diameter of 2.45 cm and thickness of 0.5 mm. The electrolyte was produced in the laboratory and composed of 0.8 M nickel (II) sulfate hexahydrate ( $NiSO_4 \cdot 6H_2O$ ), 0.2 M copper (II) sulfate pentahydrate ( $CuSO_4 \cdot 5H_2O$ ), and 0.28 M citric acid ( $C_6H_{10}O_8$ ). 1,4-butyne-1,3-diol ( $C_4H_6O_2$ ) content was adjusted to 2.0 g/L, 2.5 g/L, 3.0 g/L, 3.5 g/L, and 4.0 g/L.

The electroplating methods depicted in this work were performed in a high-pressure electroplating chamber, purchased from Tech Lead Enterprise Co. Ltd. (New Taipei City, Taiwan); schematics are shown in Figure 1. The chamber is made of SAE 316 grade stainless steel; the inner wall of the chamber is covered by a Teflon liner to protect against corrosion from the electrolyte; a stir bar covered in Teflon is placed inside the chamber, and the magnetic stirrer machine is on the outside of the

chamber to mix the sc-CO<sub>2</sub> with the electrolyte; after closing the chamber, the internal capacity was 180 mL. The supercritical fluid used in this study was CO<sub>2</sub> gas with 99.9% purity, purchased from C.C. Gaseous Co. (New Taipei City, Taiwan). The CO<sub>2</sub> tank is connected to a heat exchange device that cools the gas to liquefied form. The volumetric CO<sub>2</sub> concentration was around 30%. A DC power supply, model GDP-3303S, purchased from GW Instek (New Taipei City, Taiwan), was used to perform the electroplating.

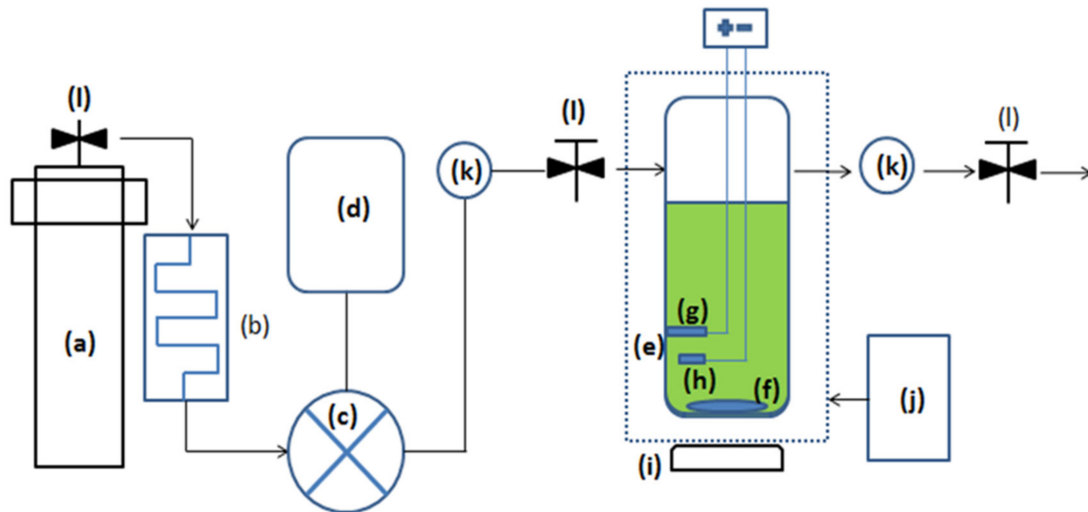


**Figure 1.** Schematics of supercritical electroplating equipment: (a) CO<sub>2</sub> tank; (b) heat exchange device; (c) high pressure pump; (d) compressor; (e) hot water lining; (f) magnetic stir bar; (g) anode; (h) cathode; (i) magnetic stirrer machine; (j) thermostatic water tank; (k) pressure gages; and (l) pressure valves.

## 2.2. Sample Preparation and Experimental Method

Brass samples were ground with sandpaper grit P800, P1500, and P2000 and sequentially polished to a mirror finish with alumina powder with particulate sizes of 1 μm, 0.3 μm, and 0.05 μm to remove surface oxide from the surface. Samples were then placed inside a glass beaker where isopropyl alcohol (IPA) was poured. The glass beaker was then placed inside an ultrasonic cleaner for five minutes. Next, IPA was poured out and acetone was poured into the glass beaker. Then it was placed again in the ultrasonic cleaner for five minutes. Finally the sample was rinsed with de-ionized (DI) water, blown dry with nitrogen gas and placed in a dry cabinet to avoid contamination. Before electroplating, one side of the sample was covered with PVC anti-plating tape. Then samples underwent pre-treatment: they were immersed in 2% NaOH solution to remove organic contaminants from the surface, and then in 35% HCl solution to activate the surface (15 s each); the sample was then rinsed in DI water, blown dry with nitrogen gas and, finally, the sample was ready for electroplating.

The sample was placed inside the high-pressure electroplating chamber, where liquefied CO<sub>2</sub> was pumped in; temperature and pressure were adjusted to achieve optimal sc-CO<sub>2</sub> electroplating parameters (pressure: 15 MPa, temperature: 50 °C) [18,19]. Magnetic agitation was started at 500 rpm for 30 minutes to allow homogenous mixing between the sc-CO<sub>2</sub> and electrolyte, then kept constant throughout the remainder of the experiment. The power supply was then connected, the desired DC values adjusted and, finally, electroplating was performed. The desired coating thickness was 50 μm. After electroplating was finished, the pressure was released to open the chamber, the sample retrieved and soaked in DI water to rinse off any remnants of electrolyte from the surface. The sample was then blown dry with nitrogen gas and stored for future analysis.

For conventional electroplating, samples underwent similar pre-treatment as described above. However there were no pressure pumping or mixing steps after the samples were placed inside the chamber. Temperature and agitation were adjusted to 50 °C and 500 rpm, respectively,

the power supply connected with the desired DC values adjusted, and electroplating was performed. The electroplating parameters are listed in Table 1.

**Table 1.** Electroplating parameters applied in this study.

Parameter	Conventional Electroplating	sc-CO <sub>2</sub> Electroplating
Pressure (MPa)	0.1	15
Temperature (°C)	50	50
Agitation speed (rpm)	500	500
Current density (A/dm <sup>2</sup> )	2.5	2.5
Surfactant content (g/L)	2.0, 2.5, 3.0, 3.5, 4.0	2.0, 2.5, 3.0, 3.5, 4.0
Plating time (h)	1	1

### 2.3. Current Efficiency Analyses

When electrical current passes through the electrolyte, the anode and cathode, respectively, undergo oxidation and reduction simultaneously, converting electrical energy into chemical energy. Cathode reactions are accompanied by hydrogen evolution, meaning current was not completely used for reduction. The current efficiency of the Cu-Ni electroplating is calculated by Equation (1) shown below:

$$\Psi = \left( \frac{2 \cdot F}{I \cdot t} \times 100 \right) \cdot \left( \frac{W_{Ni}}{58.69} + \frac{W_{Cu}}{63.54} \right), \quad (1)$$

where  $\psi$  represents current efficiency (%),  $F$  represents the Faraday constant (96,500 C/mol),  $I$  is the electrical current (A), and  $t$  is the electroplating time (s);  $W_{Ni}$  represents the weight of the Ni deposited at the cathode,  $W_{Cu}$  represents the weight of the Cu deposited at the cathode (both calculated by ion concentration in solution). The number of electrons needed for Cu-Ni ion reduction is 2.

### 2.4. Microstructural Analyses

The composition analysis of the coatings in this study was performed with a high-resolution SuperProbe Electron Probe Micro Analyzer (EPMA) model JXA-8200 by JEOL, Ltd. (Tokyo, Japan). The crystalline structure was measured by X-ray diffractometer model M03XHF by MAC Science (Yokohama, Japan), under a scanning speed of 2 deg/min, and the grain size was calculated from the main diffraction peaks by the Scherrer equation [20]. For grain size calculations, additional factors for line broadening were not considered and the results achieved are used as qualitative descriptions of the trends rather than a precise quantitative tool. Precise measurements should consider the effects of micro-twins, stacking faults, uniform stresses, etc. Microstructural surface morphology was observed by field emission scanning electron microscope (FESEM), model Sigma Essential by Zeiss Microscopy GmbH (Jena, Germany). Surface roughness ( $R_a$ ) was measured using  $\alpha$ -step profilometer model Surfcoeder SEF3500 by Kosaka Laboratory Ltd. (Tokyo, Japan) and interpreted by the accompanying software.

### 2.5. Internal Stress Analyses

Internal stresses can seriously affect the quality of coatings. Internal stresses in the coatings form due to unbalanced crystallization during the plating process. There are five main factors in the creation of internal stresses: (1) crystalline joining; (2) hydrogen penetration; (3) co-plating of foreign substances; (4) excess energy; and (5) lattice defects [21].

For this work, internal stresses were calculated using a laser displacement setup to measure the bending of substrates after electroplating. The substrate used for this analysis was a rectangular slab of Cu with dimensions 30 mm × 7 mm × 0.1 mm. Samples were placed on top of an XY moving table, where a single point was measured at a time. The laser sensor shoots a beam at the surface to determine differences in height relative to a reset point. The data were then introduced into SigmaPlot<sup>®</sup> software (Version 11.0, Systat Software Inc., San Jose, CA, USA) to plot a graph, which was curve-fitted by linear

regression to calculate the radius of curvature ( $R$ );  $R$  was then inserted into the Stoney equation to calculate internal stresses, as shown in Equation (2) below:

$$\sigma_f = \frac{E_s \cdot t_s^2}{6(1 - \nu_s)Rt_f'} \quad (2)$$

where  $\sigma_f$  is the calculated internal stress in the coating;  $E_s$  and  $\nu_s$  are the material's Young's modulus and Poisson ratio, respectively;  $R$  is the calculated radius of curvature;  $t_s$  and  $t_f$  are the thicknesses of the substrate and coating, respectively. Quantification of internal stresses by this method has been previously reported [22].

## 2.6. Electrochemical Analyses

In this work electrochemical analysis was performed via potentiodynamic polarization scanning (PPS) to obtain anodic and cathodic polarization curves for each parameter. Electrochemical experiments were performed using a potentiostat (model ECW-5000, Jiehan Technology Corp., Taichung, Taiwan) with the produced coating serving as working electrode (WE), a piece of graphite as counter electrode, and a saturated calomel electrode (SCE) as reference. Experimental parameters are shown in Table 2.

The WE was submerged into a corrosive solution and allowed to stabilize for 30 min to obtain the open circuit potential (OCP). OCP was assumed to be the corrosion potential ( $E_{\text{corr}}$ ) and a suitable range for PPS is set from  $E_{\text{corr}}$ . High  $E_{\text{corr}}$  represents low chemical reactivity, and vice versa. Through PPS, a polarization curve containing both cathodic and anodic polarization curves was obtained. From Tafel extrapolation by Cview software (Version 2.6b, Scribner Associates Inc., Southern Pines, NC, USA), the corrosion current density ( $I_{\text{corr}}$ ) can be calculated. Finally, from the  $I_{\text{corr}}$  we can estimate the material corrosion rate. Measurement of the electrochemical properties by this method was reported in a previous study [22]; theoretical concepts of Tafel analysis and examples of typical polarization curves can be found in the literature [23].

**Table 2.** Parameters for the electrochemical experiment performed in this study.

Parameter	Setting
Exposed area of WE	1 cm <sup>2</sup>
Plated thickness	50 μm
OCP stabilization time	30 min
Scanning potential	Vs. reference SCE
PPS speed	1 mV/s
PPS range	Dependent on OCP: ±250 mV (Total scan range: 500 mV)
Corrosive solution	3.5% NaCl
Temperature	20 °C ± 2 °C

## 3. Results and Discussion

### 3.1. Current Efficiency (CE) Analyses

The CE was calculated by measuring the sample's weight before and after electroplating. Results are shown in Figure 2. The CE of the conventional process was ~65%, and the CE of the sc-CO<sub>2</sub> process was approximately 56%. Secondary reactions waste electrical charge, reducing the entire process efficiency [24], however, the CE of the conventional process was ~10% higher than the sc-CO<sub>2</sub> process due to dissolved CO<sub>2</sub> in solution, which lowers the CE even further. However, CE was evidently improved by the addition of even a small quantity of 1,4-butyndiol for both processes. 1,4-butyndiol is known to undergo hydrogenation under a sc-CO<sub>2</sub> environment [25], so it is possible that the surfactant could bind with extra H<sup>+</sup> that initially reduced the current efficiency of the plating processes. Furthermore, a steady flat line was achieved when increasing the surfactant

content to 3.0 g/L; we believe this is a sign of quasi-saturation of the surfactant in solution. Further increasing the surfactant content might overcome the saturation condition and help to absorb  $H^+$  again. However, after increasing surfactant content to 4.0 g/L and over, steady drop of current efficiency was observed; further increases of surfactant content did not significantly affect the current efficiency, which could be attributed to the inability of the electrolyte to dissolve more surfactant after achieving complete saturation.

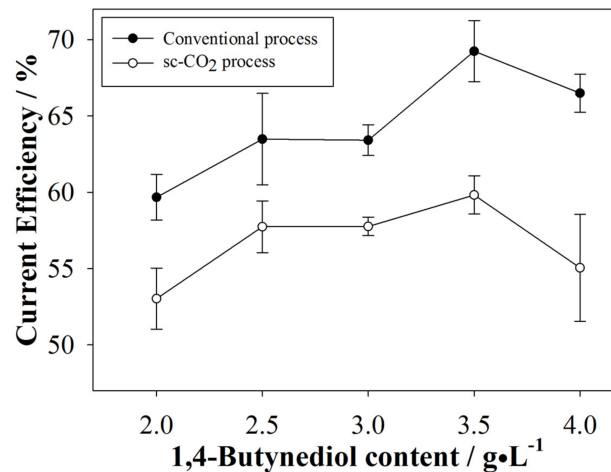


**Figure 2.** Comparison of the CE between the conventional and sc-CO<sub>2</sub> electroplating.

### 3.2. Microstructural Analyses

#### 3.2.1. Nickel Content of the Plated Coatings

The elemental contents and composition of the plated coatings as measured by EPMA are shown in Figure 3. Since it is a costly and time-consuming analysis, EPMA measurement was performed only once per sample. As stated above, the addition of 1,4-butynediol to the emulsified electrolyte reduced excess  $H^+$  in solution, disabling their ability to remain at the cathode surface; therefore, the produced coatings were relatively more densely packed. This becomes evident from SEM observations which will be discussed later (see details in Section 3.2.3). From Figure 3 we also infer real surfactant saturation was achieved at 2.5 g/L, because further increasing the surfactant content no longer significantly affected the Ni content on the coatings.

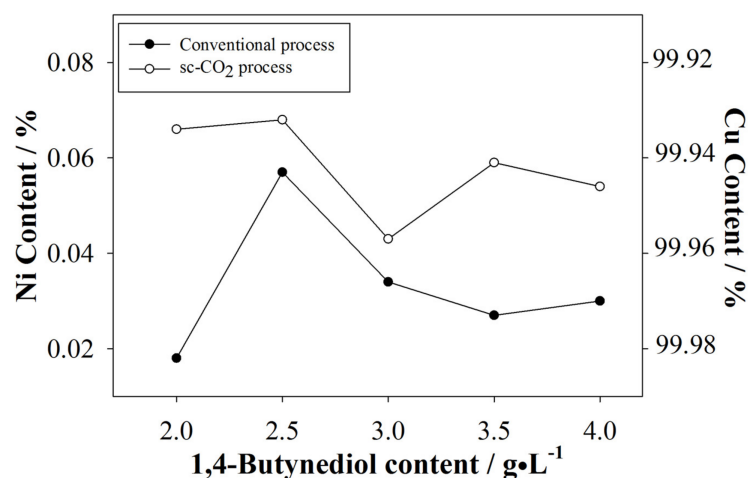


**Figure 3.** Comparison of Ni content between the conventional and sc-CO<sub>2</sub> electroplating.

### 3.2.2. Average Grain Size of the Plated Coatings

The usual factors that affect the deposition mechanism include applied current density, Ni ion concentration, and surfactant content in the electrolyte. Increases in current density are known to effectively decrease crystallite size, and vice versa. Ni ion concentration is known to affect polarization because it provides enhanced mass transfer [6]. The sc-CO<sub>2</sub> environment is also known to affect the deposition mechanism due to the effect similar to pulse plating [14]. However, for this specific study, current density and Ni ion concentration remained fixed throughout the experiment, reducing the number of affecting factors. The sc-CO<sub>2</sub> parameters chosen were the optimal parameters found from previous studies [17–19,22], thus, their deposition mechanism was understood. Differences in surfactant content are seen to affect the crystalline structure of coatings, shifting the intensity of the measured peaks. Crystallographic orientations were measured by X-ray diffraction (XRD) for sc-CO<sub>2</sub> and conventional processes and are shown, respectively, in Figures 4 and 5. For both cases the strongest peak was in the (111) orientation located at ~43°, with slight signals in the (200) and (220) directions, evidence of face-centered cubic (fcc) structures. Since the produced coatings had an overall higher Cu content compared to Ni, they were compared to an elemental Cu XRD reference pattern. Regardless of the electroplating process or surfactant content, the preferred orientation remained unchanged. No detectable peaks of impurities were found. However, the shifts observed from the elemental Cu pattern to the measured XRD patterns were most likely due to co-plating with Ni.

Coatings produced by the sc-CO<sub>2</sub> process were expected to have smaller grain sizes and, indeed, peak broadening was observed from coatings produced by the sc-CO<sub>2</sub> process, hinting to the relatively smaller grain sizes. The calculated results are shown in Figure 6. The sc-CO<sub>2</sub> process under optimal parameters should always result in coatings with smaller grain sizes compared to the conventional process. Extra H<sup>+</sup> in the solution is attracted to the substrate surface carrying the negative potential, which causes momentary passivation of the substrate's surface; thus, no electroplating occurs. Metal ions attach to the substrate surface and commence nucleation. The sc-CO<sub>2</sub> mixed with the electrolyte reacts with the extra H<sup>+</sup> forming carbonic acid, and effectively removes H<sup>+</sup> from the substrate surface. New metal ions can attach to the substrate's surface. These processes occur continuously, resulting in alternating on-off periods. At the chosen pressure, plating on time is short and leads to higher surface concentration of the metal ions, restricting grain growth. 1,4-butyndiol is also known to react with hydrogen at high pressures [26]; thus, more H<sup>+</sup> could be removed from the substrate surface. Increasing surfactant content affects the on-off periods, restricting grain size even further. However, on-off periods were disturbed over the threshold of 2.5 g/L and, thus, we see from Figure 6 that the grain size increased once again.

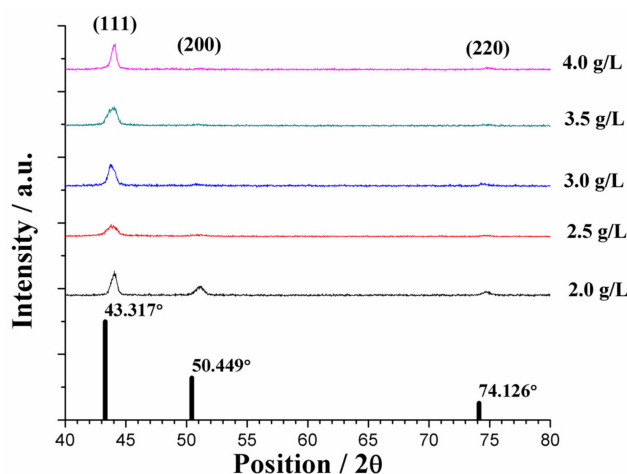


**Figure 4.** XRD peaks of the conventional process under various surfactant content levels. The reference patterns of elemental Cu (ICDD# 01-085-1326) are shown as black bars.

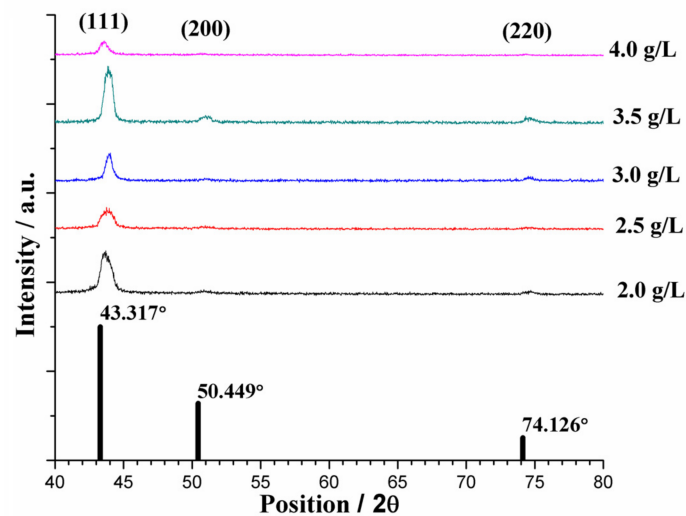


**Figure 5.** XRD peaks of the sc-CO<sub>2</sub> process under various surfactant content levels. The reference patterns of elemental Cu (ICDD# 01-085-1326) are shown as black bars.

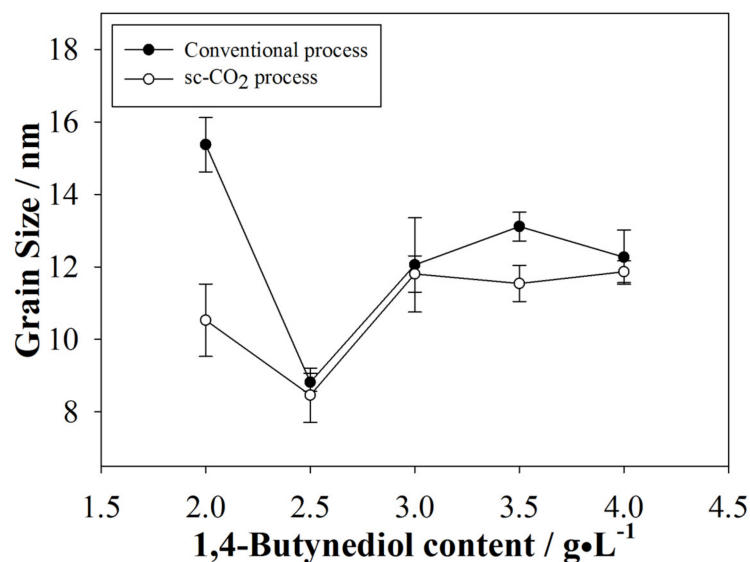


**Figure 6.** A comparison of the grain size between the conventional and sc-CO<sub>2</sub> processes.

### 3.2.3. Surface Morphology of the Plated Coatings

Coating surface morphologies plated by conventional and sc-CO<sub>2</sub> processes were observed by FESEM. Representative figures that show the effects of the process and surfactant concentration were selected and are shown in Figure 7. Coatings produced by the sc-CO<sub>2</sub> process were smoother than those produced by the conventional process and presented fewer defects. The addition of the surfactant is able to reduce excess H<sup>+</sup> that would otherwise attach to the substrate's surface. Sc-CO<sub>2</sub> is known to possess high solubility with hydrogen, so it was expected that surface morphology in the sc-CO<sub>2</sub> process becomes smoother for near-saturation concentrations, and vice versa. Figure 7a shows the film produced by the conventional method with 2.0 g/L of surfactant. The morphology is random and uneven with visible dark patches. However, this is not as evident in Figure 7b, which shows the film produced by the sc-CO<sub>2</sub> method with 2.0 g/L of surfactant. There were no large, dark patches, suggesting enhanced coverage of the surface. Dark patches in SEM images represent areas with poor adhesion where the coating has peeled off (thought to be the case in Figure 7a) or areas of low



conductivity (such as oxides) which do not allow electrons to bounce back to the SEM detector properly, similar to the case of Figure 7b.

Figure 7c shows the film produced by the conventional method with 2.5 g/L of surfactant, which was the optimal concentration for many of the characteristics described previously. It is clearly observed that the crystal growth was more ordered and structured. This could be attributed to the reduction of excess  $H^+$  in the electrolyte. Moreover, Figure 7d shows the film produced by the sc-CO<sub>2</sub> process with 2.5 g/L of surfactant, which displayed the smallest grains observed in this study. At similar scales, the size of grains is clearly smaller in the coating produced by the conventional process or in those produced by the sc-CO<sub>2</sub> process with various surfactant contents, which supports the results observed from Figure 6. In contrast, excess  $H^+$  was absorbed relatively easily by the substrate surface in conventional plating, creating more pinholes and defects.

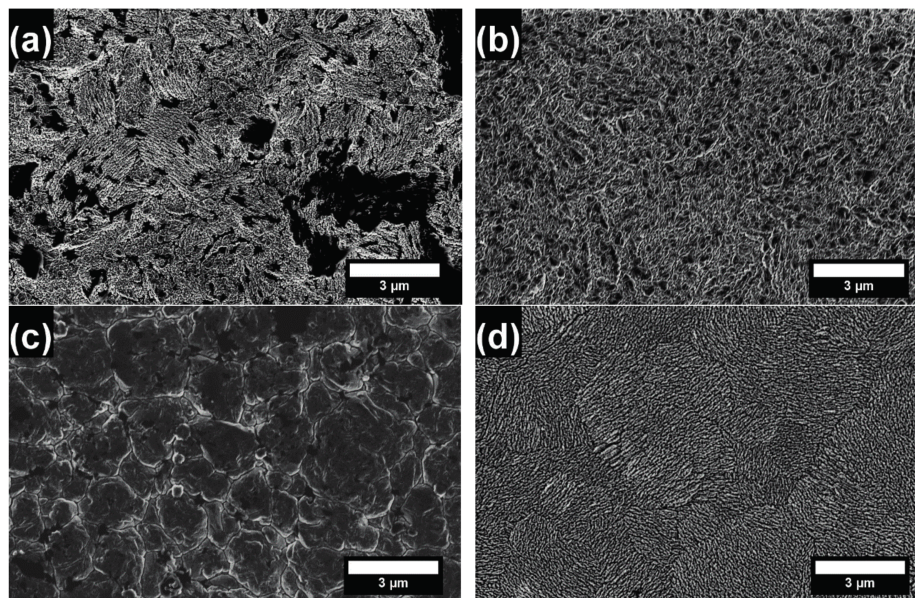


**Figure 7.** Representative SEM images of coating surface morphologies fabricated by the conventional and sc-CO<sub>2</sub> processes at different surfactant content levels: (a) conventional and (b) sc-CO<sub>2</sub> processes with 2.0 g/L 1,4-butanediol; and (c) the conventional and (d) sc-CO<sub>2</sub> process with 2.5 g/L 1,4-butanediol.

#### 3.2.4. Surface Roughness of the Plated Coatings

Average  $R_a$  was measured by an  $\alpha$ -step profilometer and the results are shown in Figure 8. From Figure 7 it was seen that morphology of coatings produced by the conventional process contained relatively more defects, thus, the average  $R_a$  is expected to be higher than for coatings produced by the sc-CO<sub>2</sub> process. Roughness of coatings with near saturation surfactant content are expected to be lower and, indeed, a trend similar with the results described above was observed.

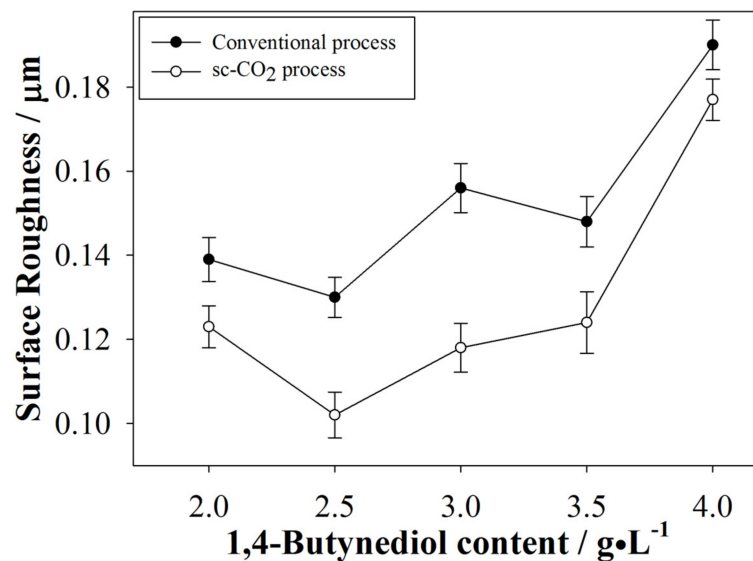


**Figure 8.** Comparison of surface roughness between the conventional and sc-CO<sub>2</sub> processes.

### 3.3. Internal Stress of the Plated Coatings

The calculated internal stresses of coatings produced in this study are shown in Figure 9. The internal stresses found in coatings produced by the sc-CO<sub>2</sub> process were lower than those found in the conventional process. During the conventional process, excess H<sup>+</sup> in solution attached to the substrate surface, leaving behind voids and compressive stresses after electroplating was completed. In the sc-CO<sub>2</sub> process, CO<sub>2</sub> in the solution removed excess H<sup>+</sup> from the surface, effectively reducing voids and internal stresses. Additionally, we observe a similar, but inverse, relationship between surfactant content with internal stress relative to that with grain size, which is expected. Reduced grain size should, indeed, present increased internal stresses; however, addition of surfactant with the sc-CO<sub>2</sub> process generally reduced internal stress compared to the conventional process. Moreover, we infer that the compositions, crystal structures, and local orientations were inconsistent when co-plating different metals, changing the volume of the coating, and exerting influence over the degree of internal stresses.

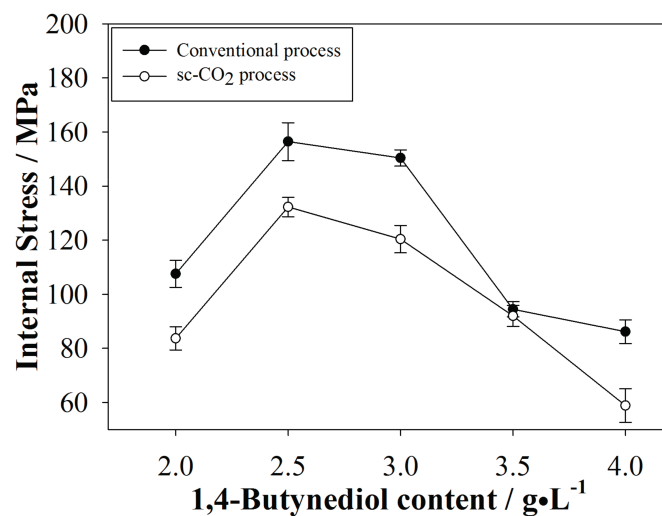


**Figure 9.** Internal stresses calculated from coatings fabricated by the conventional and sc-CO<sub>2</sub> processes.

### 3.4. Electrochemical Properties of the Plated Coatings

The oxidation speed of Ni is inherently low, therefore, insertion of even small quantities of Ni into Cu deposits effectively enhance its electrochemical properties. Moreover, a common application of 1,4-butyndiol in industry is as an additive to increase the corrosion resistance of coatings [26]. Cu-Ni coatings were produced by conventional and sc-CO<sub>2</sub> processes with various surfactant contents, and electrochemical properties were analyzed by PPS. From Section 3.2.1 we know that Cu content was the highest, therefore, pure Cu coatings were also analyzed for comparison. Representative polarization curves are shown in Figures 10 and 11.

Figure 10 shows the polarization curve of a set of coatings produced with 2.5 g/L of surfactant content by the various processes. This specific surfactant content resulted in better mechanical properties on the previously discussed analyses, so enhanced electrochemical resistance was also expected. Pure Cu coatings produced by the conventional method displayed poor electrochemical resistance ( $-0.366$  V,  $2.50$   $\mu\text{A}/\text{cm}^2$ ), which promoted the motivation for this study. Cu-Ni coatings under the conventional process slightly improved the electrochemical resistance as hinted by the relatively higher  $E_{\text{corr}}$  and  $I_{\text{corr}}$  measured ( $-0.342$  V,  $6.89$   $\mu\text{A}/\text{cm}^2$ ); however, coatings produced by the sc-CO<sub>2</sub> process evidently had even better electrochemical resistance ( $-0.198$  V,  $28.56$   $\mu\text{A}/\text{cm}^2$ ).

Figure 11 shows the polarization curves of a set of coatings produced with 3.0 g/L of surfactant content by the various processes. Similarly, pure Cu coatings by conventional process displayed the lowest electrochemical resistance ( $-0.368$  V,  $0.99$   $\mu\text{A}/\text{cm}^2$ ), Cu-Ni coatings by the conventional process displayed slightly better electrochemical resistance ( $-0.352$  V,  $5.42$   $\mu\text{A}/\text{cm}^2$ ) and Cu-Ni coatings by the sc-CO<sub>2</sub> process displayed an even better electrochemical resistance ( $-0.257$  V,  $4.49$   $\mu\text{A}/\text{cm}^2$ ). Additionally, electrochemical resistance of coatings produced with 3.0 g/L surfactant content was inferior to those produced with 2.5 g/L surfactant content. Similar results were observed for analysis with lower or higher surfactant contents. This is attributed to the saturation condition discussed in the previous sections. For all cases, electrochemical resistance of Cu-Ni coatings exceeded that of pure Cu coatings regardless of the electroplating process used.

Moreover, a passivation region was observed for coatings produced by the conventional process but not for coatings produced by the sc-CO<sub>2</sub> process. The passivation region is where  $I_{\text{corr}}$  kept relatively constant and low, which hints to the formation of barrier films causing drops in  $I_{\text{corr}}$ . The breakdown of barrier films occurred when  $E_{\text{corr}}$  increased, but pitting corrosion becomes an issue from this point onward. Additionally, pinholes and defects significantly increase the possibility of localized corrosion, so the Cu-Ni coatings fabricated by the sc-CO<sub>2</sub> process were expected to display higher electrochemical resistance compared to those produced by the conventional process.

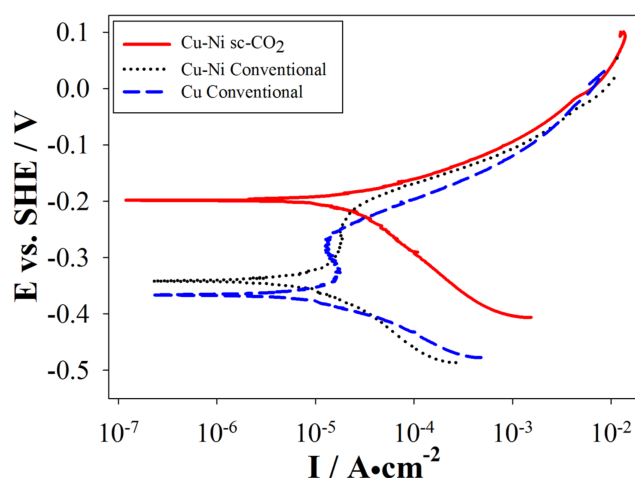
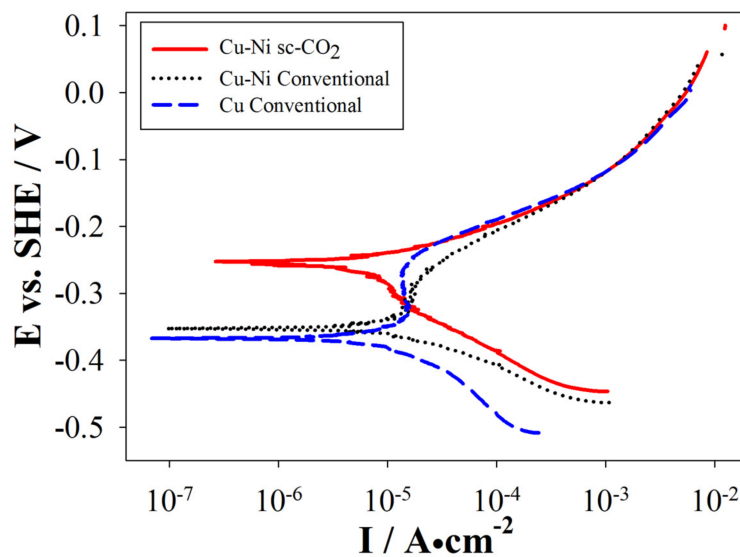


Figure 10. Potentiodynamic polarization curve of a sample fabricated with 2.5 g/L surfactant content.



**Figure 11.** Potentiodynamic polarization curve of a sample fabricated with 3.0 g/L surfactant content.

#### 4. Conclusions

This work reports the fabrication of Cu-Ni alloy co-plating with 1,4-butyne-1,3-diol as a surfactant in sc-CO<sub>2</sub> electroplating at low DC settings. Smaller grains resulted in brighter and smoother coatings produced by the sc-CO<sub>2</sub> process. Saturation of the surfactant content was achieved at 2.5 g/L, a point where evident changes were observed for all of our experiments. 1,4-butyne-1,3-diol undergoes hydrogenation under the sc-CO<sub>2</sub> environment and, thus, the surfactant could bind with free hydrogen ions in solution that normally reduced current efficiency. Lower or higher surfactant concentrations did not significantly affect Ni content on the coatings, nor the current efficiency of the process. The process described in this study effectively reduced pinholes normally caused by residual H<sup>+</sup> on the coating's surface through an effect similar to pulse plating and the hydrogen-binding capabilities of the surfactant. Moreover, application of the sc-CO<sub>2</sub> process with added surfactant effectively reduced the coating roughness and the degree of internal stress when compared to the conventional process. A preferred crystal orientation of the Cu-Ni coatings was observed and remained in the (111) direction regardless of the process used, which verifies that surfactant content did not affect crystal orientation. Finally, coatings produced by the sc-CO<sub>2</sub> process with surfactant displayed relatively less localized corrosion compared to the conventional process with surfactant due to a lower incidence of pinholes, as seen from the PPS experiments.

This study has laid the groundwork for further research on alloy co-plating and future goals in our research group include more detailed descriptions on the deposition mechanisms due to the interactions of the added surfactant.

**Acknowledgments:** The authors express gratitude to Chun-Ying Lee and his research group at the department of Mechanical Engineering, National Taipei University of Technology for providing insight on manufacturing processes, technical support, and equipment. The authors also gratefully acknowledge support for this work by the Ministry of Science and Technology of Taiwan under contract number MOST 104-2221-E-027-052.

**Author Contributions:** H.-C.C., J.S. and H.-Y.C. designed the experiments. H.-Y.C. performed the experiments. H.-Y.C. and J.S. analyzed the data and wrote the manuscript. H.-C.C. supervised, reviewed, and edited the manuscript where appropriate.

**Conflicts of Interest:** The authors declare no conflict of interest.

## References

1. Ghosh, S.K.; Grover, A.K.; Dey, G.K.; Suri, A.K. Synthesis of Corrosion-resistant Nanocrystalline Nickel-copper Alloy Coatings by Pulse-plating Technique. *Defence Sci. J.* **2005**, *55*, 63–74. [[CrossRef](#)]
2. Wang, S.H.; Guo, X.G.; Yang, H.Y.; Dai, J.C.; Zhu, R.Y.; Gong, J.; Peng, L.M.; Ding, W.J. Electrodeposition mechanism and characterization of Ni-Cu alloy coatings from eutectic-based ionic liquid. *Appl. Surf. Sci.* **2014**, *288*, 530–536. [[CrossRef](#)]
3. Kear, G.; Barker, B.D.; Stokes, K.; Walsh, F.C. Electrochemical Corrosion Behavior of 90–10 Cu-Ni Alloy in Chloride-based Electrolytes. *J. Appl. Electrochem.* **2004**, *34*, 659–669. [[CrossRef](#)]
4. Baskaran, I.; Sankara Narayanan, T.S.N.; Stephen, A. Pulsed electrodeposition of nanocrystalline Cu–Ni alloy films and evaluation of their characteristic properties. *Mater. Lett.* **2006**, *60*, 1990–1995. [[CrossRef](#)]
5. Alper, M.; Kockar, H.; Safak, M.; Baykul, M.C. Comparison of Ni-Cu alloy films electrodeposited at low and high pH levels. *J. Alloys Compd.* **2008**, *453*, 15–19. [[CrossRef](#)]
6. Desislava, G.; Avdeev, G.; Rashkov, R. Electrodeposition and characterization of Ni-Cu alloys. *Surf. Coat. Technol.* **2014**, *240*, 204–210.
7. Nguyen, V.C.; Lee, C.Y.; Chang, L.; Chen, F.J.; Lin, C.S. The relationship between nano crystallite structure and internal stress in Ni coatings electrodeposited by watts bath electrolyte mixed with supercritical CO<sub>2</sub>. *J. Electrochem. Soc.* **2012**, *159*, 393–399. [[CrossRef](#)]
8. Li, Y.W.; Yao, J.H.; Huang, X.X. Effect of Saccharin on the process and properties of nickel electrodeposition from sulfate electrolyte. *Int. J. Metall. Mater. Eng.* **2016**, *2*, 123.
9. Atanassov, N.; Bozhkov, H.; Vitkova, S.; Rashkov, S. Morphology and properties of nickel plate deposited in the presence of butynediol. *Surf. Technol.* **1982**, *17*, 291–299. [[CrossRef](#)]
10. Guo, X.G.; Li, X.M.; Zheng, Y.H.; Lai, C.; Li, W.L.; Luo, B.B.; Zhang, D.X. Effects of surfactants on high regularity of 3D porous nickel for Zn<sup>2+</sup> adsorption application. *J. Nanomater.* **2014**. [[CrossRef](#)]
11. Tsai, W.L.; Hsu, P.C.; Hwu, Y.; Chen, C.H.; Chang, L.W.; Je, J.H.; Lin, H.M.; Groso, A.; Margaritondo, G. Building on bubbles in metal electrodeposition. *Nature* **2002**, *417*, 139. [[CrossRef](#)] [[PubMed](#)]
12. Yoshida, H.; Sone, M.; Mizushima, A.; Abe, K.; Tao, X.T.; Ichihara, S.; Miyata, S. Electroplating of Nanostructured Nickel in Emulsion of Supercritical Carbon Dioxide in Electrolyte Solution. *Chem. Lett.* **2002**, *11*, 1086–1087. [[CrossRef](#)]
13. Yoshida, H.; Sone, M.; Mizushima, A.; Yan, H.; Wakabayashi, H.; Abe, K.; Tao, X.T.; Ichihara, S.; Miyata, S. Application of Emulsion of Dense Carbon Dioxide in Electroplating Solution with Nonionic Surfactants for Nickel Electroplating. *Surf. Coat. Technol.* **2003**, *173*, 285–292. [[CrossRef](#)]
14. Yoshida, H.; Sone, M.; Mizushima, A.; Abe, K.; Tao, X.T.; Ichihara, S.; Miyata, S. The effects of dense carbon dioxide on nickel plating using emulsion of carbon dioxide in electroplating solution. *Surf. Coat. Technol.* **2004**, *182*, 329–334.
15. Chiu, S.Y.; Chung, S.T.; Lin, C.Y.; Tsai, W.T. Electrodeposition of Ni-Al<sub>2</sub>O<sub>3</sub> composite coatings employing supercritical CO<sub>2</sub> baths. *Surf. Coat. Technol.* **2014**, *247*, 68–73. [[CrossRef](#)]
16. Berche, B.; Henkel, M.; Kenna, R. Critical phenomena: 150 years since Cagnaird de la Tour. *Rev. Bras. Ens. Fis.* **2009**, *31*. [[CrossRef](#)]
17. Chuang, H.C.; Hong, G.Y.; Sanchez, J. Fabrication of high aspect ratio copper nanowires using supercritical CO<sub>2</sub> fluids electroplating technique in AAO template. *Mater. Sci. Semicond. Process.* **2016**, *45*, 17–26. [[CrossRef](#)]
18. Chuang, H.C.; Lai, W.H. Fabrication of through-silicon vias by supercritical CO<sub>2</sub> emulsion-enabled nickel electroplating. *Mater. Sci. Semicond. Process.* **2014**, *23*, 27–33. [[CrossRef](#)]
19. Chuang, H.C.; Lai, W.H.; Sanchez, J. An investigation of supercritical-CO<sub>2</sub> copper electroplating parameters for application in TSV chips. *J. Micromech. Microeng.* **2014**, *25*, 015004. [[CrossRef](#)]
20. Weil, R. Origins of Stress in Electrodeposits Pt. 2: Review of the Literature Dealing with Stress in Electrodeposited Metals. *Plating* **1971**, *58*, 50–56.
21. Nguyen, V.C.; Lee, C.Y.; Chen, F.J.; Lin, C.S.; Liu, T.Y. Study on the internal stress of nickel coating electrodeposited in an electrolyte mixed with supercritical carbon dioxide. *Surf. Coat. Technol.* **2012**, *206*, 3201–3207. [[CrossRef](#)]

22. Chuang, H.C.; Teng, Y.C.; Sanchez, J. Study on the effects of pressure and material characterization in thin film and TSV fabricated by supercritical carbon dioxide electrolyte. *Mater. Sci. Semicond. Process.* **2016**, *56*, 5–13. [[CrossRef](#)]
23. Badea, G.E.; Caraban, A.; Sebesan, M.; Dzitac, S.; Cret, P.; Setel, A. Polarisation measurements used for corrosion rates determination. *J. Sustain. Energy* **2010**, *1*, 83–87.
24. Tsai, W.T.; Chuang, Y.C. Effect of surfactant on the electrodeposition of Ni–P coating in emulsified supercritical CO<sub>2</sub> baths. *Thin Solid Films* **2013**, *529*, 322–326.
25. Kriaa, K.; Serin, J.P.; Contamine, F.; Cézac, P.; Mercadier, J. 2-Butyne-1, 4-diol hydrogenation in supercritical CO<sub>2</sub>: Effect of hydrogen concentration. *J. Supercrit. Fluids* **2009**, *49*, 227–232. [[CrossRef](#)]
26. European Chemical Agency. But-2-Yne-1,4-Diol Summary Risk Assessment Report. Available online: <https://echa.europa.eu/documents/10162/d25f048d-21b9-4949-a7c6-7d9ae3a1aa3a> (accessed on 11 April 2017).



© 2017 by the authors. Licensee MDPI, Basel, Switzerland. This article is an open access article distributed under the terms and conditions of the Creative Commons Attribution (CC BY) license (<http://creativecommons.org/licenses/by/4.0/>).